Bull Volcanol (2004) 66:1–14
DOI 10.1007/s00445-003-0291-0

RESEARCH ARTICLE

S. A. Soule · K. V. Cashman · J. P. Kauahikaua

Examining flow emplacement through the surface morphology of three rapidly emplaced, solidified lava flows, Kīlauea Volcano, Hawai'i

Received: 30 April 2002 / Accepted: 28 March 2003 / Published online: 19 September 2003

Abstract The surface morphologies (pāhoehoe and ʻaʻā) of three short-duration, high effusion rate Kīlauean lava flows record important information about basaltic lava flow emplacement. Variations in the distributions of surface morphology with distance from the vent indicate the cumulative effects of both intrinsic (i.e. composition, temperature, crystallinity) and extrinsic (i.e. topography, effusion rate, flow velocity) parameters of emplacement. Detailed surface mapping with aerial photos and radar imagery reveal that all three flows exhibit a flow facies evolution common to Hawaiian ʻaʻā flows of (1) pāhoehoe sheet flows, (2) ʻaʻā-filled channels within pāhoehoe sheets, and (3) channelized ʻaʻā. The resulting surface morphology distribution is similar among flows, although differences in the length scale of the distribution exist. We characterize the surface morphology distribution by the distance from the vent to the onset of the surface morphology transition (0.5–4 km) and the length of the transition from onset to completion (1.5–7 km). The parameters that affect surface morphology changes are investigated by comparison of two recent flows (July and December 1974). There is no correlation between the location of the surface morphology transition and local changes in slope; instead, ʻaʻā formation initiates when flows reach a critical groundmass crystallinity of φ~0.18. This critical crystallinity, composed primarily of plagioclase and pyroxene microlites, does not appear to be affected by the presence or absence of olivine phenocrsyts. This crystallinity also correlates with theoretical and experimental predictions for the onset of a yield strength and supports the idea that crystal-crystal interactions are controlled primarily by the content of prismatic crystals (e.g. plagioclase). The dependence of the morphologic transition on post-eruptive crystallization requires that the down-flow location of the surface morphology transition is determined by both eruption temperature and effusion rate, with hotter, faster flows traveling greater distances before crystallizing enough to form ʻaʻā. The length of the transition zone is proportional to the rate of flow cooling, which is dramatically influenced by topographic confinement. A comparison of the surface morphology distributions of these flows to the 1823 Keaiwa flow, which has a similar composition, pre-eruptive topography, and eruption temperature suggests that it was emplaced at effusion and flow advance rates, 300 m^3/s and 1–3 m/s, respectively, typical of observed Hawaiian eruptions and much lower than previous estimates from the run-up height of lava. Evaluation of independent methods to determine flow-front velocities indicates that run-up height estimates consistently exceed estimates from tree-mold measurements and observation of active flows of <2 m/s. Channel velocities of 1–3 m/s, inferred through analysis of ʻaʻā clinker size as a function of distance from the vent, are higher than those inferred at the flow-front.

Keywords Kîlauea · ʻaʻā Flow · Surface morphology · Channels · Crystallinity

Editorial responsibility: J. Stix

S. A. Soule (✉) · K. V. Cashman
Department of Geological Sciences,
1272 University of Oregon,
Eugene, OR, 97403-1272, USA
e-mail: ssoule@gladstone.uoregon.edu
Tel.: +1-541-346-5987
Fax: +1-541-346-4692

J. P. Kauahikaua
Hawaiian Volcano Observatory,
Hawai'i Volcanoes National Park,
P.O. Box 51, Hilo, HI, 96718-0051, USA

Introduction

Basaltic lava flows pose a threat to human activity that can be mitigated by understanding how flows are emplaced. Most important for hazard assessment and mitigation are estimates of the effusion rates, flow advance velocities, and flow lengths that might be anticipated in future eruptions (e.g. Pinkerton and Wilson 1994; Wadge et al. 1994). While easily determined for

observed eruptions, these parameters are more difficult to infer from solidified flows that represent a much larger fraction of the eruptive history of most volcanoes. For this reason, it is important to develop methods for inferring emplacement conditions from older, solidified lava flows.

Active basaltic flows produce two fundamentally different surface morphologies, pāhoehoe and ‘a‘ā, that can be linked to different rates and mechanisms of flow advance (e.g. Macdonald 1953; Peterson and Tilling 1980). Pāhoehoe flows form lobes, sheets, or toes. Given a steady supply of lava pāhoehoe flows will advance discontinuously as a thickening crust restricts lateral spreading, and subsequently fails. ‘A‘ā flows typically form channels, and advance continuously as little resistance to flow is provided by the continuously brecciating crust. Flows classified as ‘a‘ā often result from high effusion rates (Rowland and Walker 1990) and advance rapidly in their early stages—thus they pose the greater risk to those living near volcanic vents. In Hawai’i, flows that advance as ‘a‘ā usually form pāhoehoe surfaces near the vent. The resulting transition from pāhoehoe to ‘a‘ā has long fascinated observers of Hawaiian lava flows (Wentworth and Macdonald 1953; Macdonald 1953; Peterson and Tilling 1980) because of its potential to record flow conditions.

Here, we link the flow-scale surface morphology evolution of two short-lived ‘a‘ā flows from Kīlauea to the conditions of their emplacement. As surface morphology is affected by local conditions such as topography, effusion rate, and flow velocity, as well as physical properties of the lava, we attempt to quantify both these extrinsic and intrinsic parameters of emplacement. We then relate the surface morphology distribution to emplacement parameters such as flow advance velocity, channel velocity, etc., which we then use to infer emplacement conditions of a third flow. The excellent preservation of surface features on these flows also allows us to examine the process of channel formation and development in the early stages of ‘a’ā flow field development.

Flow observations

This study focuses on three lava flows from Kīlauea volcano erupted in July 1974, December 1974, and 1823. Each was erupted from a fissure vent, had a short duration, and displays a heterogeneous surface morphology. Two of the flows erupted near Kīlauea’s summit caldera (July and December 1974) whereas the third (Keaiwa 1823) erupted at the coast, along Kīlauea’s southwest rift zone (Fig. 1). Eyewitness accounts and descriptions of the emplacement of the 1974 flows are found in Lockwood et al. (1999). Ellis (1825) provides secondhand accounts of the emplacement of the Keaiwa 1823 flow and Stearns (1926) describes the solidified flow.

Each flow preserves two distinct surface morphologies, pāhoehoe and ‘a‘ā (Dutton 1884; Macdonald 1953).

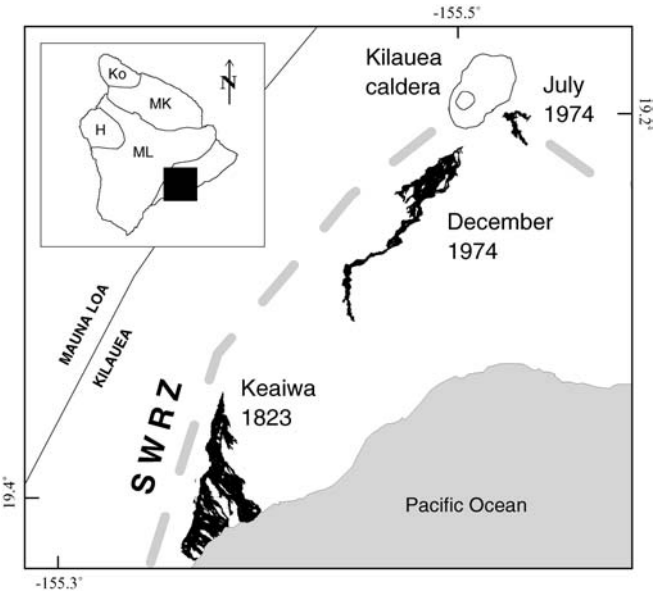

Fig. 1 Map showing location of July 1974, December 1974, and Keaiwa 1823 flows on Kīlauea Volcano. The December 1974 and Keaiwa 1823 flows are located along Kīlauea’s southwest rift zone (*SWRZ*). The July 1974 flow is located near the origin of the ERZ. *Inset* shows study area (*black box*) relative to Mauna Loa (*ML*), Mauna Kea (*MK*), Hualalai (*H*), and Kohala (*Ko*) volcanoes

Pāhoehoe flow surfaces change systematically with distance of flow away from the vent. Shelly pāhoehoe is common near eruptive vents and is characterized by large gas cavities between the upper crust and the flow core (Swanson 1973). Slabby pāhoehoe has a smooth surface and a thick ($\geq$5.5 cm) crust broken into plates ranging in size from 0.1 to >1 m^2 (Jones 1943). Pasty pāhoehoe (also called toothpaste pāhoehoe by Rowland and Walker 1987) is found at a greater distance from the vent and has a rough, hackly crust that deforms into either ropey folds or flat, broken plates (Nichols 1939). ‘A‘ā flow surfaces are rough and composed of individual clinkers torn or broken from the lava surface. Transitional ‘a‘ā first appears at the margins of incipient channels as spiny clinkers that often contain patches of smooth crust (e.g. Guest et al. 1987). ‘A‘ā covers the medial to distal portions of each flow with large clinkers characterized by rough, spinose, and granular surfaces (e.g. Macdonald 1953).

July 1974

The July 1974 flow (J74) erupted in two distinct episodes from elongate fissures located to the north and south Keanakāko’i crater (Fig. 2a). We focus on the eruption that produced the southern flow, which began on July 19 at 1230 h Hawaiian Standard Time (HST) with fire fountaining along the E-W trending fissures. Spectacular tree molds preserved on the flow record a maximum flow height 3 m above the current flow surface and were used by Moore and Kachadorian (1980) to calculate a flow-

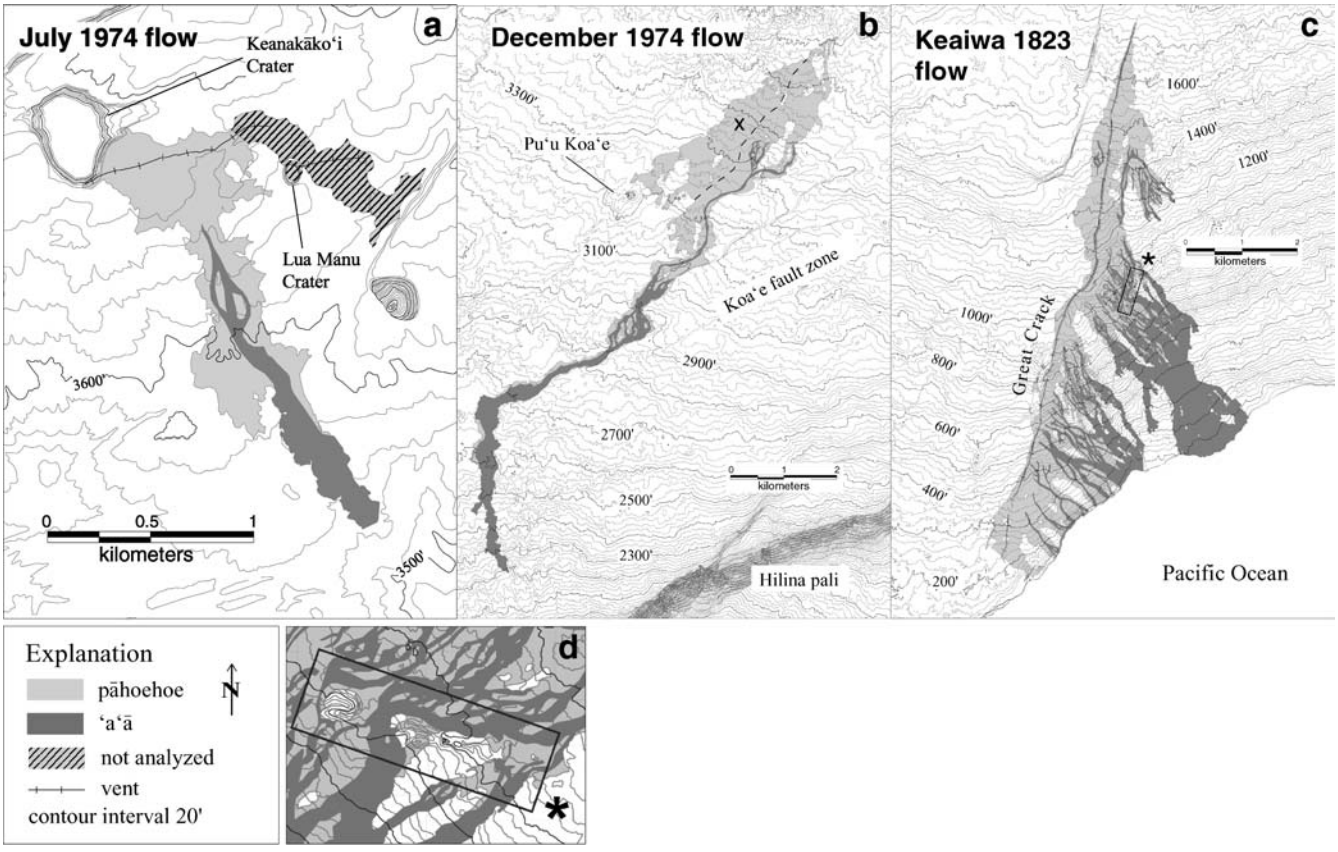

Fig. 2 Maps showing vents, flow field, and surface morphologies of the **a** southern July 1974, **b** December 1974, and **c** Keaiwa 1823 flows. Pāahoehoe, shown in *light gray*, includes shelly, slabby and pasty pāhoehoe. 'A'ā, shown in *dark gray*, indicates the location of channels on the flows. We do not analyze the portion of the July 1974 flow fed primarily by a set of vents E of Lua Manu Crater. The vents feeding the December 1974 flow opened chronologically from the NE to the SW. Flow was focused by scarps of the Koa'e fault zone. The area marked '*x*' on the Dec. 1974 flow indicates the region of flow that may not have contributed material to the dominant flow path, and was excluded when calculating an alternate surface morphology distribution for this flow. The Keaiwa 1823 flow was erupted from the Great Crack and truncated by the ocean at lengths of 0.5–7 km. The lava plastered cones of Stearns (1926) are marked '*' in **c** and shown in more detail in **d**

front velocity of 1.6 m/s near the vent and 0.1 m/s at its distal end. Slabby pāhoehoe appears within ~300 m of the vent and dominates the next 200 m of flow length. At 0.5 km from the vent a single channel, identified by transitional 'a'ā along the channel margins, forms in the central part of the flow. This channel bifurcates around a small topographic high, then reforms into a single channel that persists for the length of the flow. The 'a'ā-filled channel is flanked by pāhoehoe to 1.7 km from the vent, beyond which the flow is entirely 'a'ā. The eruption lasted 3–5 h at an average effusion rate (Q) of 150–275 m^3/s, producing a total flow length just over 2 km and flow volume of ~3.5×10^6 m^3.

December 1974

The December 1974 (D74) flow began at 0256 h HST on December 21 with 40-m-high fire fountains forming along a series of right-stepping NE-SW fissures. Fire fountaining initiated at the NE end of the fissure system, migrated to the SW, and concluded ~6 h later at an average $Q\approx270$ m^3/s for a volume of ~5.9×10^6 m^3 (Lockwood et al. 1999). The proximal 3 km of the flow is a wide expanse of shelly pāhoehoe interrupted by numerous kīpuka (Fig. 2b). Pāhoehoe sheets advanced rapidly (1.4–2.2 m/s; Lockwood, personal communication 2000) to the SW over Keanakāko'i ash units. The first morphological transition at ~0.5 km from the vent is marked by slabby pāhoehoe found on the up-flow side of kīpuka, at breaks in slope, and along boundaries between large, continuous pāhoehoe sheets. At a similar distance, pasty pāhoehoe wells up from cracks and is exposed where large pāhoehoe sheets pull apart. The first channels are apparent at ~4 km from the vent, marked by transitional 'a'ā along their margins. The great width of the proximal flow (~2.5 km) resulted in the formation of several distinct channels that focus into a single channel where the flow encounters Koa'e fault scarps. Channels are flanked by narrow pāhoehoe margins that persist for 10 km of the 12 km flow length. In the medial portion of the flow these pāhoehoe margins predate channel development and mark the maximum extent of the pāhoehoe advance (~8 km). Farther down flow, pasty pāhoehoe

breakouts emerge from the ʻaʻā channel. The distal portion of the flow advanced as ʻaʻā at a rate of <0.3 m/s to its terminus 12.4 km from the vent (Lockwood, personal communication 2000).

Keaiwa 1823

The Keaiwa flow (K1823) erupted in 1823 at the distal end of Kīlauea's subaerial southwest rift zone (SWRZ) from a 10 km long fissure known as the "Great Crack" (Fig. 2c). Localized fountaining emplaced low spatter deposits and lava balls along the vent (Stearns 1926). The flow advanced to the SE as wide pāhoehoe sheets that created numerous kīpuka. Slabby and pasty pāhoehoe appear within 500 m of the vent, accompanied by transitional ʻaʻā along channel margins. The great length of vent from which the lava issued resulted in the formation of ~50 individual channels which focus into 5–10 main channels down flow. Some channels in the medial portion of the flow make sharp (~90°) turns to accommodate topographic barriers formed by older spatter cones. These cones are covered with a thin veneer of K1823 lava (the "lava plastered cones" of Stearns 1926) and have been used to infer a flow front velocity of 15 m/s and an effusion rate of 21,000 m^3/s (Baloga et al. 1995; Guest et al. 1995). The flow entered the ocean at distances varying from 0.15–7.0 km from the fissure.

Methods

To characterize flow emplacement we described the surface morphology characteristics of the flow, properties of the flow environment, and physical properties of the lava. We used aerial photos and radar images to map flow surface morphologies. Topographic maps and DEMs provided information on the slopes over which the flows moved. We conducted field work to ground-truth surface morphology maps, collect samples for analysis, and make qualitative and quantitative observations of flow features. Finally, we determined the glass temperature and crystallinity of the lavas to evaluate changes in lava rheology with transport distance.

Flow surface mapping

The distribution of pāhoehoe and ʻaʻā surface morphologies were mapped from differences in reflectivity on aerial photos of the D74, J74, and K1823 flows. We digitized flow boundaries and morphologic units (pāhoehoe and ʻaʻā) from geospatially registered photos to produce surface morphology maps, which were ground-truthed to assess their accuracy. To determine morphological changes with flow distance we analyzed slices of the surface morphology maps sampled perpendicular to flow direction where possible. A similar characterization of surface morphology can be obtained from radar imagery, where signal value corresponds to surface roughness (Campbell 2002). The results from the two methods are nearly identical, with slight differences due to our classification of transitional surface morphologies (pasty and slabby pāhoehoe) as pāhoehoe, whereas they are classified as ʻaʻā on radar images (Gaddis et al. 1990).

We analyzed topography using 7.5′ topographic quadrangles (USGS 1981). Topographic profiles along dominant flow paths (as indicated by lava channels) and slope maps created from 30-m DEMs were used to calculate, respectively, slope along the flow path and local gradients.

Field methods

Field studies included verification of surface morphology maps, characterization of channel development, flow sampling, and measurement of features that preserve information on rates of flow advance. In an approach similar to Anderson et al. (1998) we investigated channel evolution by measuring the size of pāhoehoe plates and ʻaʻā clinkers along transects across the channel at multiple down-flow locations. Pāhoehoe plates are best characterized by three separate measurements (x, y, z), while ʻaʻā clinkers are approximated as rotational ellipsoids (characterized by maximum and minimum axes). When possible we measured every plate and clinker across a transect, but for very wide channels (>60 m) measurements were made at regularly spaced intervals (e.g., measure 2 m, skip 5 m). As a control, we measured one transect using three different interval spacings with similar results indicating that measuring at intervals rather than across the entire channel imposes no apparent sampling bias.

To characterize the evolution of the physical properties of the lava (temperature and crystallinity) we sampled glassy flow surfaces at sub-equal spacings along each flow or along primary channels (e.g. K1823). We collected glass from all surface morphologies present at each sample site to determine the range of physical properties that characterize the lava at each location.

Flow-front velocity has been estimated by measuring lava run-up heights (e.g. Guest et al. 1995; Kauahikaua et al. 2002). Run-up occurs when lava flows onto an obstacle in the flow path (Fig. 3). These features are generally preserved only in pāhoehoe, and in the flows studied are found only in the proximal region of the D74 and K1823 flows. We measured run-up height from the top of the preserved local flow surface to the maximum height of fluid lava on the obstacle (the height reached by lava crust can be mm to cm higher due to piling-up of fragments). As flow advance is usually most rapid near the vent, and as flow degassing and draining of the molten core could increase the apparent height difference, velocities estimated from run-up heights are maxima.

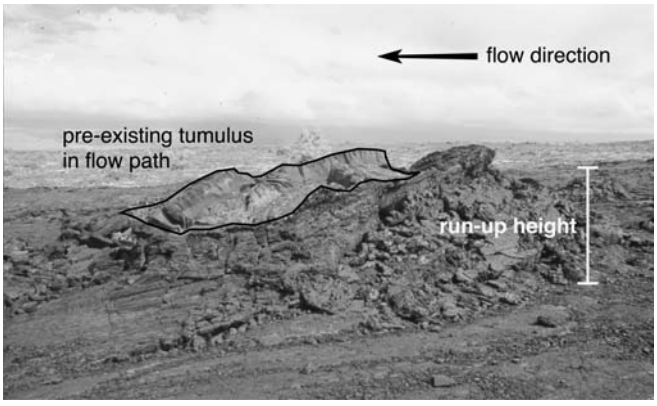

Fig. 3 Near vent run-up locality on the Keaiwa 1823 flow. Pre-existing tumulus is outlined in black. Flow direction is to the left. Run-up height (~1.6 m) is measured from the preserved local flow surface and does not include upper 0.02 m which represents crust pushed above the level of liquid lava

Analytical techniques

All phases preserved in glassy samples were analyzed using a Cameca SX-50 electron probe microanalyser (EPMA) at the University of Oregon. Analysis conditions included an accelerating voltage of 15 kV, 10 nA beam current, and a 10-μm spot size to reduce Na loss in glass (a 3–5 μm spot size was used for crystalline phases). We analyzed at least ten glassy areas on each sample for all major oxide components and reduced data using the PAP data reduction routine (Pouchou and Pichoir 1991; Table 1). We used similar methods to determine crystal compositions in five to nine samples per flow for use in mass balance calculations.

We determined the quench temperature of each sample with a MgO-glass geothermometer calibrated for Kīlauean lavas by Helz and Thornber (1987). Developed on lavas from the Kīlauea Iki lava lake, this technique has been applied most often to water quenched samples from active flows (Cashman et al. 1994; Helz et al. 1995; Cashman et al. 1999; Folley 1999). However, Clague et al. (1999) used this technique on air quenched samples from solidified lava flows to determine the thermal efficiency of tubes feeding the ʻAilaʻau eruption (A.D. 1445). As temperatures are based on the rate of MgO consumption from the fluid by the crystalline phases, we assume that the crystallinity is in equilibrium with the temperature of emplacement. Due to the possibility of small kinetic lag times in crystallization, glass temperatures are maxima.

We determined syn-emplacement increases in groundmass by (1) mass balance calculations using vent glass and crystalline phase compositions, and (2) point counts of backscattered electron (BSE) images collected on a JEOL 6,300 V scanning electron microscope with an accelerating voltage of 10 kV and a 15-mm working distance. After applying a correction factor to convert mass to volume fraction crystals, both techniques produced similar results. Total crystallinities of the D74 lavas are higher than mass balance results due to ~0.07 pre-eruptive, skeletal olivine microphenocrysts that are present in the vent lavas and thus not accounted for by mass balance based on initial glass composition.

Results

Surface morphology distribution

In all flows, the fraction of flow surface covered by pāhoehoe (*P*) decreases systematically with distance from the vent (Fig. 4). This distribution can be fit by a sigmoidal curve that describes three morphologic zones. An isomorphic pāhoehoe zone (*P*=1.0–0.97) reflects the emplacement of pāhoehoe sheet flows near the vent. This is followed by a transition zone (*P*=0.97–0.03), the beginning of which marks the first appearance of ʻaʻā in

Table 1 Representative glass analyses for each flow. Average of ten spot analyses of glass from air-quenched proximal (pahoehoe) and distal (aa) lava samples from each flow. Glass temperatures are calculated using MgO content (Helz and Thornber 1987). Phase proportions for July 1974 and December 1974 flows are calculated using analyzed phase compositions from each flow and mass balance calculations, while Keaiwa 1823 phase proportions are obtained from point-counting BSE images

	July 1974		December 1974		Keaiwa 1823	
	Proximal	Distal	Proximal	Distal	Proximal	Distal
SiO_2	50.07	50.13	50.32	50.76	50.18	50.88
TiO_2	2.58	3.00	2.56	2.91	2.64	2.89
Al_2O_3	13.79	12.92	13.30	13.28	13.69	13.63
FeO*	11.38	12.87	11.35	11.97	11.41	11.73
MnO	0.19	0.22	0.18	0.17	0.14	0.19
MgO	6.72	5.63	7.58	5.73	6.60	5.97
CaO	10.91	10.49	11.16	10.71	11.34	10.78
Na_2O	2.34	2.34	2.29	2.23	2.26	2.44
K_2O	0.51	0.61	0.48	0.54	0.50	0.53
P_2O_5	0.26	0.31	0.26	0.27	0.26	0.26
Total	98.75	98.52	99.47	98.56	99.01	99.31
MgO T (°C)	1,151	1,127	1,167	1,131	1,148	1,135
Volume fraction						
Glass	1.0	0.79	0.95	0.79	–	0.77
Olivine	<0.01	0.03	0.01	0.05	–	0.01
Pyroxene	<0.01	0.07	0.03	0.09	–	0.10
Plagioclase	<0.01	0.11	0.01	0.07	–	0.12

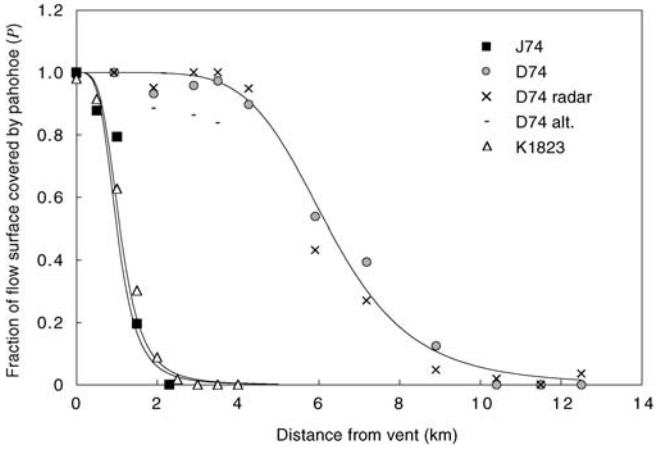

Fig. 4 Plot of fraction of flow surface covered by pāhoehoe (*P*) vs. distance from the vent (km) for the July 1974 (*J74*), December 1974 (*D74*), and Keaiwa 1823 (*K1823*) flows. Each displays a similar pattern of surface morphology distribution characterized by an isomorphic pāhoehoe zone, a transitional zone, and an isomorphic ‘a‘ā zone. D74 data collected from radar images (x) shows good agreement with air-photo data. An alternate set of D74 measurements using only a portion of the proximal flow (-) bracket the location of the transition zone onset

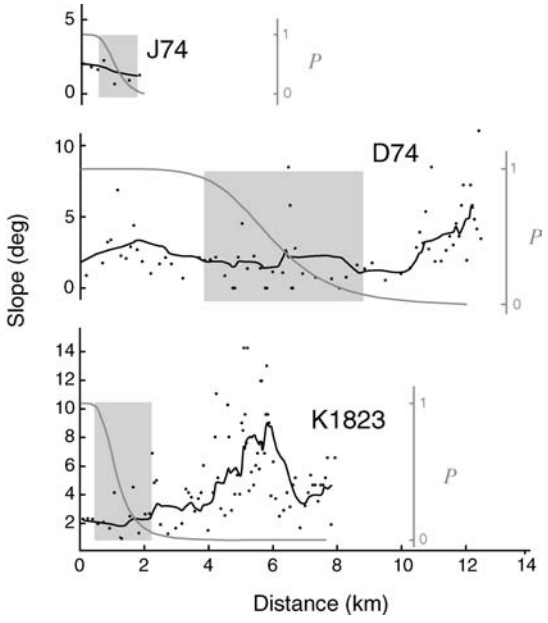

Fig. 5 Slope over which the July 1974 (*J74*), December 1974 (*D74*), and Keaiwa 1823 (*K1823*) flows traveled calculated from USGS topographic maps. *Solid black line* shows moving average of five data points. Superimposed surface morphology distribution curves (*solid gray line*) indicate the area in which the morphology transition occurs (*gray box*). Average slope within this region is <5° for each flow

channels within wide pāhoehoe sheets. The fraction of pāhoehoe declines as channels widen and the bounding pāhoehoe narrows. Finally, an isomorphic ‘a‘ā zone (*P*=0.0–0.03) marks the farthest down-flow location of pāhoehoe, beyond which lavas advance as ‘a‘ā.

Errors in surface morphology distribution are assessed by comparing morphology distributions measured at different resolutions (i.e., slice widths). Errors are small at either end of the distribution curve (less than ±0.03 *P*), but can be as large ±0.1 *P* in the transition zone. Linear regressions of *P* vs. distance in the transition zone show that R^2 decreases with increasing resolution as smaller slice widths amplify the importance of small anomalies (regions of excess pāhoehoe or ‘a‘ā). Slice widths of 0.5–1 km minimize these perturbations but provide sufficient data to define distribution patterns.

Although patterns of surface morphology distribution are similar in all three flows, the onset and extent of the transition zone is variable. In the J74 and K1823 flows, the transition zone begins at 0.5 km from the vent and spans a distance of 1 km. In contrast, the transition zone on the D74 flow begins ~4 km from the vent and spans ~5 km of flow length. Uncertainty in the location of the transition onset in the latter flow arises from ambiguity in whether the main branch of the flow is fed by the entire eruptive fissure. Thus, we define a range of transition zone onset distances of 3–4.5 km by measuring the surface morphology distribution on the entire flow and on only the part of the flow fed from the easternmost part of the main fissure (Fig. 4b).

To assess the role of pre-existing topography in generating differences in surface morphology distribution, we compared the underlying slope of each flow. The average slope for all three flows within and above the transition zone is gentle (<5°) (Fig. 5). Abrupt increases in slope at the distal end of the D74 and K1823 flows (10–20°) have no effect on surface morphology as both flows have already transitioned to ‘a‘ā. Some channels do initiate at local increases in slope (5–10°) on both the D74 and K1823 flow; however, in general, the location of the surface morphology transition does not appear to correlate directly with changes in slope.

Lava temperature and crystallinity

The intrinsic properties of lava (temperature and crystallinity) play an important role in determining surface morphology (Cashman et al. 1999). We examined the relationship of lava temperature to both surface morphology and distance (cooling rate) to evaluate the effect of changing lava rheology on surface morphology.

The highest glass temperatures on each flow are found in near-vent spatter and shelly pāhoehoe samples. Maximum quench temperatures are 1,168 °C for the D74 flow and ~1,150 °C for both the J74 and K1823 flows. Temperature decreases systematically with distance from the vent at a rate of 6±1 °C/km in both the J74 and K1823 flows (Fig. 6). The D74 flow shows a more complex cooling history. Vent samples contain olivine phenocrysts and a maximum temperature of 1,168 °C. Glass temperatures indicate cooling to 1,145 °C within ~2 km of the vent, an average cooling rate of 13.4 °C/km. A wide range of temperatures in vent samples implies that different

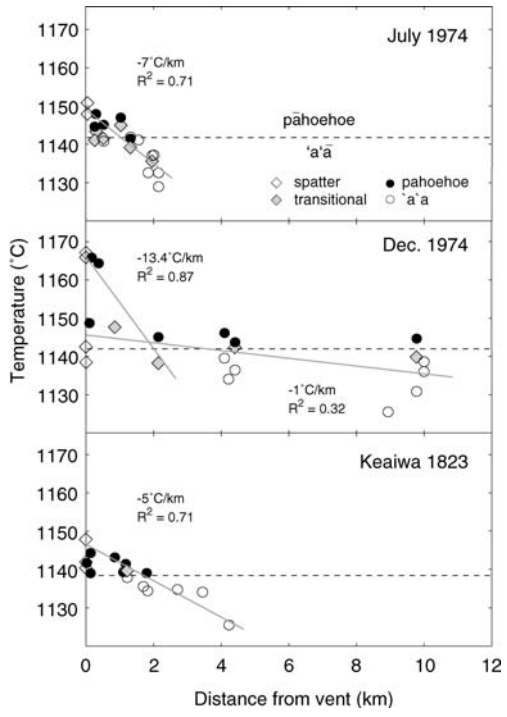

Fig. 6 MgO temperature (Helz and Thornber, 1987) vs. distance from the vent for the July 1974, December 1974, and Keaiwa 1823 flows. Symbol height represents average uncertainty in glass temperature (i.e., 1σ of MgO wt% from microprobe analyses). Linear regression of the data yields spatial cooling rates of 6.0 and 5.8 °C/km for the J74 and K1823 flows. The D74 flow shows rapid cooling near the vent (~13 °C/km), and slower cooling (~1 °C/km) after that. The *dashed line* marks the boundary between pāhoehoe and ʻaʻā at 1,140±1 °C

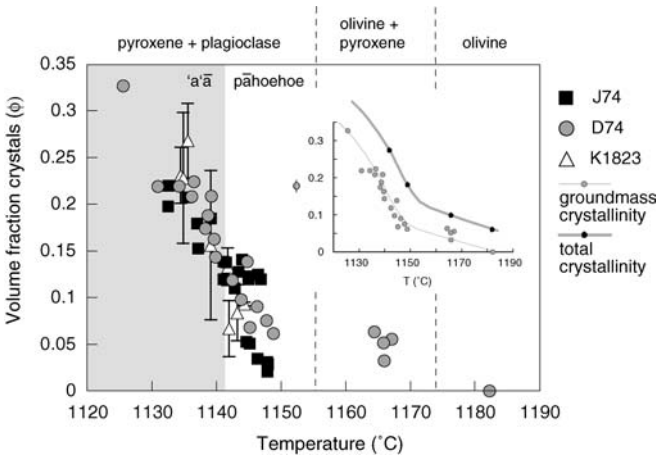

Fig. 7 Groundmass crystallinity vs. temperature of samples from the July 1974 (*J74*), December 1974 (*D74*), and Keaiwa 1823 (*K1823*) flows. Crystallinities for the J74 and D74 flows were determined by mass balance corrected for density differences between the crystals and glass and verified by point counting of BSE images. Crystallinities for the K1823 flow were determined by point counting, and *error bars* indicate the observed ranges of crystallinities. Crystallizing phases are shown above the temperature range in which they are observed. *Inset* shows difference between groundmass and total crystallinity of the D74 flow resulting from the presence of <0.07 pre-eruptive olivine microphenocrysts

parts of the flow may have erupted at different temperatures, thus this cooling rate should be considered a maximum. Decreased cooling (1 °C/km) is evident from the medial to the distal portion of the D74 flow.

Lava temperature also varies as a function of sample morphology with spatter, pāhoehoe, transitional, and ʻaʻā samples showing decreasing average temperatures respectively. Each morphology preserves a range of glass temperatures, with the range of spatter and transitional samples overlapping those of both pāhoehoe and ʻaʻā. However, in all flows there is a clear temperature break at 1,140±1 °C between pāhoehoe and ʻaʻā.

The observed decrease in glass temperature results in an increase in groundmass crystallinity (φ) (Fig. 7). J74 and K1823 lavas were erupted at 1,150 °C nearly crystal free (φ<0.01), and subsequently crystallized plagioclase and pyroxene at a rate of 0.017 φ/°C. D74 lavas were erupted with some olivine microphenocrysts (φ<0.07) and crystallized pyroxene and olivine at 0.001 φ/°C between 1,168 °C and 1,150 °C. Below ~1,150 °C (the eruption temperature of the J74 and K1823 flows), however, plagioclase began to crystallize along with pyroxene and the crystallization rate increased to that of the J74 and K1823 flows at 0.017 φ/°C.

Flow advance rates

Measurements of pāhoehoe run-up heights provide an estimate of proximal flow front velocities. Using simple energy conservation, the potential energy represented by lava run-up height can be converted to kinetic energy, hence velocity (e.g. Guest et al. 1995; Baloga et al. 1995; Kauahikaua et al. 2002). Run-up heights on the D74 flow range from 0.5–2.0 m with a mean of 1.2 m. Measurements on the K1823 flow have slightly higher values of 1.5–4.0 m, with a mean of 2.3 m (Fig. 8). Neither flow shows a correlation between run-up height and distance from the vent. Mean flow-front velocities estimated from these values are 4.7 and 6.1 m/s for the D74 and K1823 flows, respectively. The inferred flow front velocity for the D74 flow is approximately twice the maximum observed value of 2.2 m/s. The mean run-up height (and inferred flow front velocity) for the K1823 flow is substantially lower than the maximum apparent run-up height of 11 m (and estimated velocity of 15 m/s) measured on the lava plastered cones (Guest et al. 1995). These discrepancies suggest that flow front velocities inferred from run-up heights should be evaluated in the context of other flow emplacement data.

Flow channelization

Well-developed channels on long lived flows are identified by bounding levees of clinkery ʻaʻā that are often mantled by pāhoehoe overflows (e.g. Sparks et al. 1976).

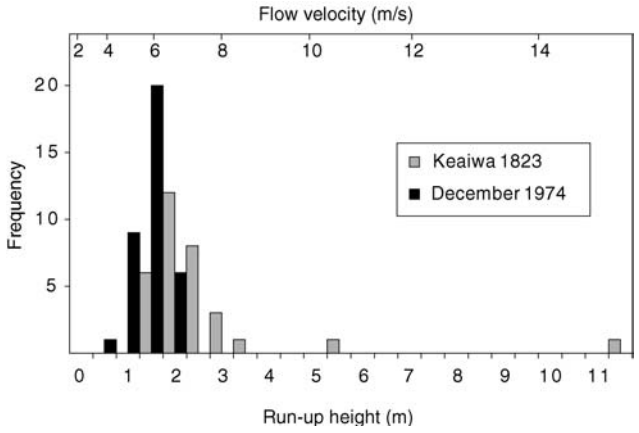

Fig. 8 Histogram of run-up heights and corresponding flow velocities measured on the December 1974 and Keaiwa 1823 flows. Measurements of 5.5 and 11.5 m represent the lava plastered cones of the Keaiwa flow and were used to infer a flow velocity of ~15 m/s (Baloga et al. 1995)

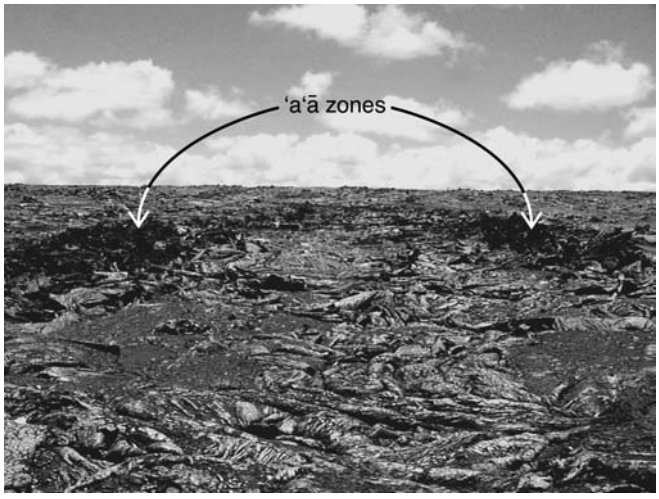

Fig. 9 Parallel ʻaʻā margins form around a central region of folded and broken pāhoehoe near a channel origin on the December 1974 flow. The ʻaʻā margins (<2 m in width) widen inward down-flow creating a dominantlyʻaʻā channel surface within 500–700 m

The incipient channels on the J74, D74, and K1823 flows, however, lack levees and are first identifiable where parallel zones of ʻaʻā form within pāhoehoe sheets (Fig. 9). Within 500–700 m of onset the parallel ʻaʻā zones expand to cover the channel with ʻaʻā, sometimes incorporating pāhoehoe plates in central regions (Kilburn 1993). Thus, channels on the short-lived flows initiate as streams of ʻaʻā lava within pāhoehoe sheets.

Measurements of fragmental material along channel transects allow us to characterize the down-channel evolution of fragment size. A decrease in average fragment size is expected if material forms at the channel origin and breaks down by mechanical interactions (Anderson et al. 1998). An increase in average size is

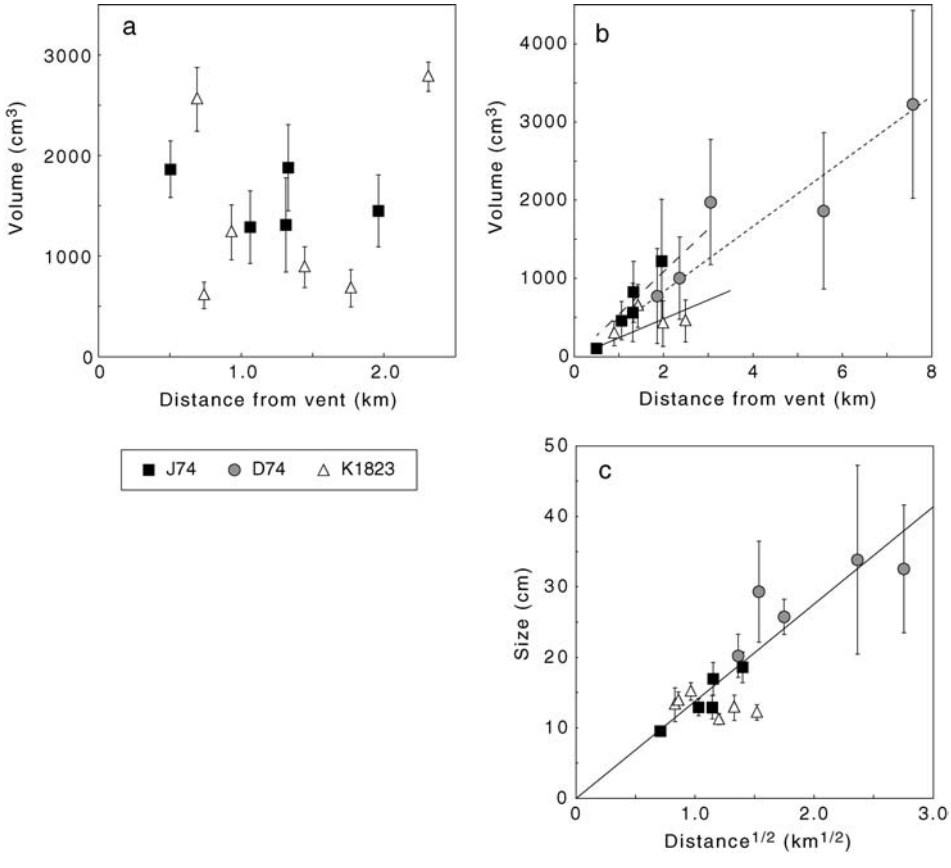

Fig. 10. a Average volume of pāhoehoe fragments with distance from vent for the July 1974 (*J74*) and Keaiwa 1823 (*K1823*) flows. **b** Average volume of ʻaʻā fragments with distance from vent for the July 1974, December 1974 (*D74*), and Keaiwa 1823 flows. **c** Average minimum axis length for largest 20% of ʻaʻā fragments at each location on all three flows. *Solid line* is linear regression fit to the data

expected if fragments are derived from gradually thickening crust or if fragment agglutination is a dominant process. The average volume of pāhoehoe plates shows no systematic change down-channel, and average thickness remains relatively constant (~4 cm; Fig. 10a). Conversely, the average volume of ‘a‘ā fragments increases with distance from the vent (Fig. 10b).

‘A‘ā clinker size is a function of original size (potentially related to crust/boundary layer thickness), mechanical breakage during transport, and agglutination of existing clinkers. Mechanically broken fragments can comprise up to 90% of material in a channel (Kilburn 1990). Agglutinated fragments are discernable by eye and composed <1% of the total material. To filter the data for processes that modify original clinker size we use the average minimum axis length of the largest ‘a‘ā size fraction (upper 20%) to represent the minimum crustal thickness at each transect location. The filtered data show a linear relationship between ‘a‘ā size and the square root of distance from the vent (Fig. 10c), as anticipated for ‘a‘ā formation from a gradually thickening crust. The relationship is well characterized by data from the D74 and J74 flows, but data from the K1823 flow show no clear trend with distance. This lack of correlation may result from the complexity of the channel system within this flow field and the tendency of channels of differing lengths to merge.

Discussion

Each flow in this study initiated as a surface-fed pāhoehoe sheet flow and subsequently forms ‘a‘ā-filled channels. This similarity in flow development is reflected in similar patterns of surface morphology distribution on each flow (Fig. 4), despite differences in spatial scale. Our quantitative analysis of the parameters affecting surface morphology (topography, temperature, and crystallinity), along with observations of the active flows (effusion and flow advance rate), allow us to explain these differences and to develop relationships among aspects of flow emplacement and surface morphology distribution. When applied to the 1823 Keaiwa flow, for which there are only secondhand accounts, these relationships allow us to place constraints on emplacement conditions, including transient parameters such as flow velocity. We analyze a number of techniques for estimating flow velocities from solidified flows to test their accuracy against observations of active flows. Finally, we examine the process of channel formation during the early stages of ‘a‘ā flow field development.

Controls on surface morphology

Both 1974 flows have a proximal pāhoehoe zone, a medial transition zone containing both pāhoehoe and ‘a‘ā, and a distal ‘a‘ā zone (Fig. 4). This pattern is typical of Hawaiian lava flows (e.g. Lipman and Banks 1987; Wolfe et al. 1988), but differs from many Etnean flows, which may be 100% ‘a‘ā at the vent (Kilburn 1990). The surface morphology distribution can be fit by an equation of the form

$$P = \frac{1}{[1 + (K \cdot d)^m]}, \quad (1)$$

where P is the fraction of the flow surface that is pāhoehoe and d is distance from the vent in kilometers. Two adjustable parameters, m and K, describe, respectively, the length scale of the transition (P=0.97–0.03) and location of the surface morphology transition onset (P=0.97). The fit parameters m and K (Table 2) can be related to conditions of emplacement.

The length of the transition from P=0.97 to 0.03 occurs over an interval of ~1.5 km in the J74 flow and ~5 km in the D74 flow. This difference reflects a greater efficiency of down-flow pāhoehoe transport in the D74 flow. Extrinsic properties of the eruption such as a high angle between the vent and flow direction, a higher initial eruption rate (Lockwood et al. 1999), and especially flow focusing (along the Koa’e fault scarps) all affect the length of the transition and potentially the length of the flow as well. Similarly, the first appearance of ‘a‘ā (the transition onset, P=0.97) occurs at ~0.5 km on the J74 flow and at ~4 km on the D74 flow. However, this difference is not explained by extrinsic parameters (e.g. pre-existing topography, average effusion rate, flow advance rate, or eruption duration) all of which are similar for the two flows. Thus, the first appearance of ‘a‘ā must be controlled by intrinsic properties of the lava.

The J74 and D74 flows were erupted at different temperatures (1,150 and 1,168 °C, respectively; Fig. 6). The higher eruption temperature of the D74 lava is consistent with its more primitive composition (Lockwood et al. 1999) and with the presence of ~0.07 olivine in near-vent lavas. In contrast, near-vent J74 lavas have only 0.01 plagioclase and pyroxene crystals. Here we use

Table 2 Surface morphology distribution fit parameters. Adjustable parameters from Eq. (<equationcite>1</equationcite>) for each flow were determined by analysis of residuals between data points and theoretical curves. Properties of the surface morphology distribution and related parameters are also listed. Transition onset occurs at P=0.97 and transition length is the distance between P=0.97 and P=0.03. T_e is the eruption temperature of the flow

Flow	m	K	Transition onset (km)	Transition zone (km)	T_e (°C)
J74	4	0.93	0.5	1.5	1,150
D74	6	0.17	3.0	5.0	1,168
K1823	4	1.00	0.5	1.5	1,149

a spatial cooling rate (°C/km) and a thermal crystallization rate (φ/°C) to compare the thermal and rheologic history of these lavas. Comparisons are made with the assumption that average velocities are similar and nearly constant. These rates can be combined to produce spatial crystallization rates for comparison to active flows and can be converted to temporal rates based on assumed flow velocities, which we will discuss later.

The proximal D74 flow cooled rapidly (13.4 °C/km) while crystallizing olivine and pyroxene at 0.001 φ/°C (Fig. 7). At ~1,150 °C, greater contributions from pyroxene and the onset of plagioclase crystallization increased the crystallization rate in the D74 flow to 0.017 φ/°C. A coincident decrease in the spatial cooling rate in this flow may represent an increase in the latent heat of crystallization (Crisp and Baloga 1994) as well as increased thermal efficiency due to confinement by topography. This is evidenced by the lower cooling rate of the D74 flow (1.0 °C/km) below ~1,150 °C, than that of the J74 flow (5.0 °C/km). Both flows crystallize plagioclase and pyroxene in sub-equal proportions at a rate of 0.017 φ/°C. Combining this with the spatial cooling rates indicates down flow increases in crystallinity at 0.02–0.09 φ/km, similar to rates observed in active open channel flows (0.05–0.08 φ/km, Kīlauea May 1997, Cashman et al. 1999; 0.01–0.04 φ/km, Mauna Loa 1984, Crisp et al. 1994).

Surface morphology is correlated with glass temperature, with no pāhoehoe found below, nor ‘a‘ā above, a critical temperature of 1,140±2 °C (Fig. 6). This temperature represents a groundmass crystallinity of 0.18±0.03 (Fig. 7), similar to crystallinities observed in transitional morphologies of other Kīlauean flows (Cashman et al. 1999; Folley 1999). As the flows advanced at similar rates, the higher eruption temperature of the D74 flow would require a longer time (flow distance) to reach the critical temperature, and hence groundmass crystallinity, of ‘a‘ā formation. Thus, the higher eruption temperature of the D74 flow accounts for the offset in the surface morphology distribution (difference in K) between the J74 and D74 flows (Table 2).

Previous estimates (Cashman et al. 1999; Folley 1999) suggest critical crystallinities of 0.35–0.40 are necessary for ‘a‘ā formation. This discrepancy may result from our sampling bias towards higher temperature samples that contain enough preserved glass for chemical analysis. As a result, we can not examine samples that have evolved beyond the initial stages of ‘a‘ā development and instead may be analyzing samples that other studies would have termed transitional. However, the critical crystallinity we identify corresponds to theoretical and experimental predictions of the onset of a yield strength for a fluid containing prismatic crystals (Hoover et al. 2001; Saar et al. 2001), which has been recognized as a common feature among ‘a‘ā flows (e.g., Cashman et al. 1999). Additionally, we find the same critical groundmass crystallinity in the D74 flow, despite the presence of 0.07 pre-eruptive, equant olivine crystals supporting the idea that yield strength is controlled by the concentration of non-equant crystals (Philpotts et al. 1998; Saar et al. 2001). Thus, our sampling, although limited to higher temperatures, has revealed that even small increases in yield strength that occur at groundmass φ~0.18 can produce ‘a‘ā-style deformation, especially at high shear rates along channel margins where many of our samples are collected.

Flow velocities

Flow velocity can have a dramatic effect on the surface morphology evolution of a flow (e.g., Peterson and Tilling 1980) and is a crucial parameter in lava flow hazard assessment (Kauahikaua et al. 1995); unfortunately, it is difficult to assess on solidified flows. Constraints on flow velocity can be made by measuring features preserved on solidified flows. For example, measurements of superelevation (Heslop et al. 1989) provide evidence for channel velocities. Measurements of run-up heights yield proximal flow-front velocities (Guest et al. 1995), and tree-mold heights can produce similar estimates along the length of a flow (Moore and Kachadorian 1980). In order to compare flow velocities on the flows in this study and to determine its effect on surface morphology we compare flow velocity estimates produced by some of the methods mentioned above and develop our own.

Flow front velocities

Flow front velocities can vary widely depending on proximity to the vent, lava temperature, local slope, and effusion rate. Moore and Kachadorian (1980) estimated the maximum velocity of the J74 flow using Jeffreys's equation solved for a Bingham fluid,

$$V = \frac{H^2 \rho g \sin\theta}{3\eta}\left[1 - \frac{\tau_y}{\tau_b} + \frac{1}{2}\frac{\tau_y^3}{\tau_b^3}\right] \quad (2)$$

where V is average velocity, H is flow thickness, θ is the angle of the ground slope, η is viscosity. The additional term indicates the degree to which the basal shear stress (τ_b) exceeds the yield strength of the lava (τ_y) (Moore and Schaeber 1975). Maximum flow thickness and ground slope are obtained from tree-molds exposed by up to 3 m of flow deflation. Using η=200 Pa s and τ_y=620 Pa, they calculated average velocities of 1.6 m/s near the vent and 0.1 m/s at the distal end of the flow.

Another method for measuring flow front velocity converts the potential energy preserved in lava run-up height (h) to a kinetic energy, hence velocity (v) by

$$v = (2gh)^{\frac{1}{2}}, \quad (3)$$

where g is the acceleration due to gravity (Guest et al. 1995). Here mass appears on both sides of the equation and thus cancels, leaving a simple balance between flow

velocity and maximum flow height. This technique consistently overpredicts flow front velocity as shown by the D74 flow, which has a mean flow-front velocity from run-up height of 4.7 m/s (Fig. 8) and an observed proximal flow-front velocity of 1.4–2.2 m/s (Lockwood, personal communication, 2000). Elevated velocity estimates are expected as run-up records only the maximum advance rate in the proximal pāhoehoe zone, and may reflect higher velocities that occur behind the flow-front where energy is not consumed by traversing colder, more irregular ground. Modification of the flow surface post-emplacement by degassing or drainage would also produce elevated velocity estimates. Additionally, debris-flow experiments suggest that velocities estimated from run-up height may exceed actual velocities by ~100% due to the formation of bow waves on the up-flow side of obstacles in the flow path (Iverson et al. 1994). As a result, we conclude that run-up height, while useful for producing relative velocity estimates between flows, does not reflect actual velocities at the flow front.

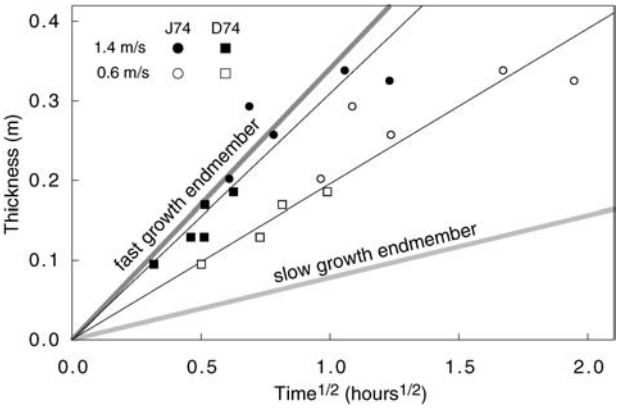

Fig. 11 Change in crustal thickness with time$^{1/2}$ for assumed channel velocities of 1.4 and 0.6 m/s for the July 1974 (*J74*) and December 1974 (*D74*) flows. End member crustal growth rates are for actively inflating (slow) and stagnant (fast) pāhoehoe flows are from Hon et al. (1993, 1994). Values near the fast growth end member (u=1.4 m/s) are favored due to greater presumed cooling rates, thus faster crustal growth rates, in ‘a‘ā flows

Channel velocities

Channelization increases the efficiency of lava transport by focusing flow, thus channel velocities may exceed flow front velocities by an order of magnitude (Lipman and Banks 1987). Whereas superelevation is a reliable method to estimate channel velocity, it requires well-developed channels with established levees that are not present on flows in this study. Additionally, this method is restricted to channel bends and determines the channel velocity at a single location on the flow, whereas channel velocities decrease dramatically with distance from the vent. Average, late-stage channel velocities may be estimated from the down-channel evolution of ‘a‘ā clinker size. The minimum thickness of ‘a‘ā fragments in channels of both 1974 flows increases linearly with the square root of distance from the vent (Fig. 10c). We can use this relationship between fragment thickness and distance to estimate transport time (i.e., flow velocity) if we assume that (1) the crust grows according to a conductive cooling model, (2) flow velocity is constant, and (3) ‘a‘ā fragments sample crustal thickness.

Crustal growth on both actively inflating and stagnant pāhoehoe flows can be modeled as

$$C = k\sqrt{t}, \tag{4}$$

where C is the thickness of the crust in meters, t is time in hours, and k is a constant related to the rate of crustal growth (Hon et al. 1993, 1994). For active inflation k=0.0799 ms$^{-1/2}$, while for stagnant flow k=0.34 ms$^{-1/2}$, with the difference resulting from the presence or absence of advective heat transfer. ‘A‘ā flows should cool more rapidly than fully crusted, inflating pāhoehoe flows due to radiative heat loss from the lava core exposed through cracks (Crisp and Baloga 1990, 1994) and minimal heat advection as crustal fragments are transported with the flow interior. Thus cooling rates estimated from clinker thickness and Eq. (4) provide maximum estimates of time (i.e., minimum cooling rates). By imposing different channel velocities (*dx/dt*) on our measure of crustal growth (*dC/dx*), we find acceptable rates of crustal growth (0.0799<k<0.34) at velocities of 0.6–1.4 m/s for both the J74 and D74 flows (Fig. 11). These velocities are minima and should increase with better estimates of crustal growth rates on ‘a‘ā flows.

Another estimate of channel velocity is obtained by assuming a cooling rate for the channelized portion of the flow core (*dT/dt*) and translating the spatial cooling rate (*dT/dx*) to a velocity (*dx/dt*). Cooling rates of ~0.005 °C/s have been measured in the proximal portions of both the Kīlauea May 1997 flow (Q=3–4 m^3/s; Cashman et al. 1999) and Mauna Loa 1984 flow ($Q\approx$100 m^3/s; Crisp et al. 1994), and thus provide an estimate of ‘a‘ā flow cooling. Using the spatial cooling rates shown in Fig. 6, a cooling rate of 0.005 °C/s suggests average channel velocities of 0.8–2.8 m/s, similar to estimates from clinker size evolution.

A compilation of all the velocity estimates (Fig. 12) shows that the two independent methods for estimating channel velocities suggest average velocities of 1–3 m/s on each flow in this study (Fig. 12). Average flow-front velocities should be less than channel velocities, which is supported estimates from tree-molds and flow observation of <~2 m/s. All estimates agree with observations of Pu‘u ‘Ō‘ō flows that share a similar morphology distribution (Wolfe et al. 1988). Estimates from run-up height consistently overlap this range, but generally overpredict velocity due to a number of possible errors including post-emplacement flow surface modification and the formation of bow-waves on the up-flow side of obstacles.

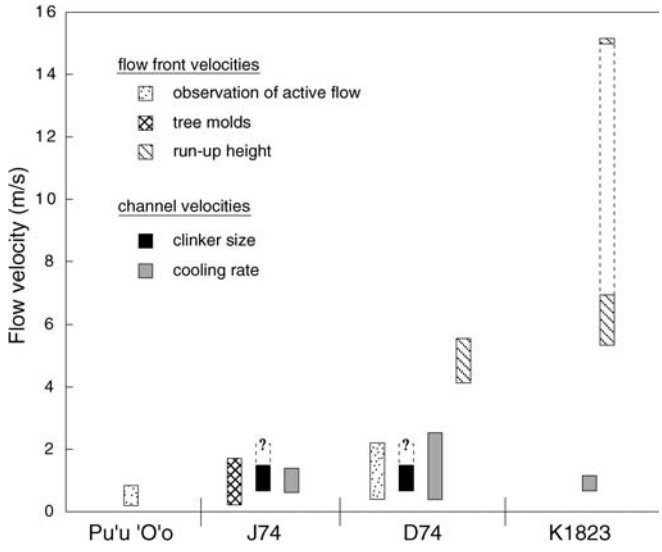

Fig. 12 Compilation of flow velocity estimates for the July 1974 (*J74*), December 1974 (*D74*), Keaiwa 1823 (*K1823*) flows and for episodes 1–20 of the Pu‘u ‘Ō‘ō eruption. *Boxes* show the range of flow velocities produced by each method. Observations of active flow are from Lockwood et al. (1999) and Wolfe et al. (1987) and describe both proximal (pahoehoe) and distal (‘a‘ā) flow front velocities. Estimates from tree-molds use a form of Jeffreys' equation to arrive at flow front velocity on the J74 flow (Moore and Kachadorian 1980). Velocity from run-up height is determined from measurements on the D74 and K1823 flow. The upper range of run-up height on the K1823 flow represents the apparent run-up on the lava plastered cones (Baloga et al. 1995), which likely reflects a different physical process. Velocity estimates from clinker size assume that ‘a‘ā clinkers reflect an increasing crustal thickness. Velocities could be greater depending on the rate of cooling in ‘a‘ā relative to pāhoehoe flows. Velocity from cooling rate uses measured cooling with distance and an assumed a cooling with time

Emplacement of 1823 Keaiwa flow

The importance of accurate flow velocity estimates from solidified flows is illustrated by the 1823 Keaiwa flow for which flow-front velocity estimates (15 m/s; Baloga et al. 1995) greatly exceed observations of Kīlauean lava flows (Wolfe et al. 1988). Part of the impetus for supporting high flow front velocities comes from this secondhand account of flow emplacement from Ellis (1825).

The people of Kearakomo also told us, that no longer than five moons ago, Pele had issued from a subterranean cavern, and overflowed the low land of Kearaara, and the southern part of Kapapala. The inundation was sudden and violent, burnt one canoe, and carried four more into the sea.

While no doubt accurately reported, inferences made from such an anecdote can be dubious. For example, the sea-cliffs along the coast at this location require that canoes be launched down ladders, a process that could take hours to complete (Langlas 1990). In addition, the location of the village relative to the vent is not known. Flow velocity decays rapidly with distance from the vent (Kauahikaua et al. in press), and if the village was located at the southern end of the flow, the distance from the vent to the ocean would be less than 0.5 km. Both facts could result in similar accounts of flow emplacement without invoking such great velocities.

The distribution of surface morphology on the Keaiwa flow closely matches that of the J74 flow, with channelization beginning 0.5 km from the vent and a complete transition to ‘a‘ā within 3 km (Fig. 4). The pre-existing topography of the K1823 flow is similar to both 1974 flows with average slopes <5° in the area in which the transition from pāhoehoe to ‘a‘ā occurred (Fig. 5). Slopes of 15° at the distal end of the flow have no additional effect on the morphology of lava that has already transformed to ‘a‘ā. The eruption temperature of the K1823 flow (1,148 °C) is also similar to the J74 flow (1,150 °C), as is its spatial cooling rate of 5.8 °C/km (Fig. 6) and T-φ relationship (Fig. 7). These similarities suggest that both the effusion rate and flow advance rate of the 1823 Keaiwa flow were also similar to the 1974 flows (200–300 m^3/s and 1–3 m/s, respectively). These effusion and flow advance rates are consistent with most observed Hawaiian lava flows, but are substantially lower than previous estimates from run-up height (21,000 m^3/s and 15 m/s; Guest et al. 1995; Baloga et al. 1995).

Our measurements of run-up height at numerous sites in the proximal and medial portions of the K1823 flow produce consistently lower flow-front velocities (~6 m/s) than those inferred by the same methods from the lava-plastered cones (15 m/s; Guest et al. 1995). Relationships between run-up and observed velocity of the D74 flow, indicate that the actual K1823 flow front velocity may have been as low as one-fifth the previous estimates. Moreover, the lava-plastered cones are in the medial part of the flow where numerous lava channels coalesced and made a right angle to flow between the two cones (Fig. 2d). The cones on the outside and inside bends of the turn have apparent run-up heights, respectively, of 11 and 5 m. Leveling data, however, show that the absolute elevation of the top of the lava veneers is the same (HVO, unpublished data 1999). This supports the interpretation of Stearns (1926) that the lava-plastered cones record the height of a lava pond that backed up behind these cones, either due to complete blockage of the flow or slowed flow as it passed through the gap. The lack of any preserved run-up within 300 m up-flow of these cones also suggests that lava may have ponded on the up-flow side.

Conclusions

The distribution of surface morphologies on a flow acts as an indicator of the cumulative effects of both intrinsic (i.e. composition, temperature, crystallinity) and extrinsic (i.e. topography, effusion rate, flow velocity) parameters of emplacement. A characteristic sigmoidal surface morphology distribution reflects a flow facies evolution common to Hawaiian ‘a‘ā flows of (1) proximal pāhoehoe sheet flows, followed by (2) ‘a‘ā filled channels within

pāhoehoe sheets, and lastly (3) channelized ‘a‘ā. Differences in the length scale of this distribution marked by the down-flow position of the surface morphology transition onset and length of the transition zone thus reflect differences in these parameters of flow emplacement.

The surface morphology transition occurs at a critical groundmass crystallinity of 0.18±0.03. Thus, given similar rates of flow advance, higher eruption temperature will result in greater distances to the transition onset. The critical crystallinity we identify matches theoretical predictions for the onset of a yield strength (Saar et al. 2001), and supports the idea that the crystal-crystal interactions (especially between non-equant plagioclase) play a large role in determining the surface morphology of a flow (Kilburn 1981; Cashman et al. 1999). Differences in the length of the transition zone seem to be controlled by extrinsic parameters such as topographic confinement and its affect on flow cooling.

Estimates of flow-front velocity from tree mold heights (Moore and Kachadorian 1980), and channel velocities from ‘a‘ā clinker size evolution and spatial cooling rate agree with observed velocities. Run-up height, the technique used to infer an extremely rapid flow advance rate for the Keaiwa 1823 flow, may provide useful relative velocities, but generally overestimates flow velocity. Similar eruption parameters and surface morphology distributions for the July 1974 and Keaiwa 1823 flow indicate that the latter was emplaced with an effusion and flow advance rate much lower than previous estimates. Large variations in flow velocity should have a dramatic effect on surface morphology (see Peterson and Tilling 1980). Further study of the shear rate dependence of the pāhoehoe to ‘a‘ā transition would facilitate better constraints on the flow dynamics from the examination of solidified flow surfaces.

The surface morphology distribution we use to assess similarities and differences in flow emplacement between flows is not always preserved on longer duration flows. Analysis of more flows with greater diversity in emplacement conditions (i.e. duration, topography, effusion rate, etc.) is needed to investigate how surface morphology distribution is affected by flow duration and to better establish the role of the parameters that effect surface morphology distribution. With further refinement, this technique may be applied the large number of solidified flows on Kīlauea, other basaltic volcanoes, and on other terrestrial planets.

Acknowledgements The authors gratefully thank the staff of the Hawaiian Volcano Observatory for logistical and material support in the undertaking of this work and Randy Cabral of Ka’u Orchards for access to their property. Scott Rowland, Steven Blake, and John Stix provided thoughtful reviews of this manuscript. Additionally, we thank colleagues, Don Swanson, Bob Tilling, Jack Lockwood, Michael Manga, and Ross Griffiths for helpful discussions. This work was supported by NSF EAR-9902851 (to K.V.C.).

References

Anderson SW, Stofan ER, Plaut JJ, Crown DA (1998) Block size distributions on silicic lava flow surfaces: implications for emplacement conditions. Geol Soc Am Bull 110:1258–1267

Baloga S, Spudis PD, Guest JE (1995) The dynamics of rapidly emplaced terrestrial lava flows and implications for planetary volcanism. J Geophys Res 100:24509–24519

Campbell BA (2002) Radar remote sensing of planetary surfaces. Cambridge University Press, Cambridge, 331 pp

Cashman KV, Mangan MT, Newman S (1994) Surface degassing and modifications to vesicle size distributions in active basalt flows. J Volcanol Geotherm Res 61:45–68

Cashman KV, Thornber C, Kauahikaua JP (1999) Cooling and crystallization of lava in open channels, and the transition of pāhoehoe lava to ‘a‘ā. Bull Volcanol 61:306–323

Clague DA, Hagstrum JT, Champion DE, Beeson MH (1999) Kilauea summit overflows: their ages and distribution in the Puna District, Hawaii. Bull Volcanol 61:363–381

Crisp J, Baloga S (1990) A model for lava flows with two thermal components. J Geophys Res 98:1255–1270

Crisp J, Baloga S (1994) Influence of crystallization and entrainment of cooler material on the emplacement of basaltic aa lava flows. J Geophys Res 99:11819–11831

Crisp J, Cashman KV, Bonini JA, Hougen SB, Pieri DC (1994) Crystallization history of the 1984 Mauna Loa lava flow. J Geophys Res 99:7177–7198

Dutton CE (1884) Geology of the Hawaiian islands. Bull Philos Soc Wash B6:13–14

Ellis W (1825) Narrative of a tour through Hawaii, or, Owhyhee. H. Fisher, Son, and P. Jackson, London, 264 pp

Fink JH, Griffiths RW (1992) A laboratory analog study of the surface morphology of lava flows extruded from point and line sources. J Volcanol Geotherm Res 54:19–32

Folley M (1999) Crystallinity, rheology, and surface morphology of basaltic lavas, Kilauea Volcano, Hawaii. MS Thesis, University of Oregon, 205 pp

Gaddis LR, Mouginis-Mark PJ, Hayashi JN (1990) Lava flow surface textures: SIR-B radar image texture, field observations, and terrain measurements. Photogramm Eng Remote Sensing 56:211–224

Griffiths RW, Fink JH (1992) Solidification and morphology of submarine lavas: a dependence on extrusion rate. J Geophys Res 97:19729–719737

Guest JE, Kilburn CRJ, Pinkerton H, Duncan AM (1987) The evolution of lava flow-fields; observations of the 1981 and 1983 eruptions of Mount Etna, Sicily. Bull Volcanol 49:527–540

Guest JE, Spudis PD, Greeley R, Taylor GJ, Baloga SM (1995) Emplacement of xenolith nodules in the Kaupulehu lava flow, Hualalai Volcano, Hawaii. Bull Volcanol 57:179–184

Harris AJL, Rowland SK (2001) FLOWGO: a kinematic thermo-rheological model for lava flowing in a channel. Bull Volcanol 63:20–44

Helz RT, Thornber CR (1987) Geothermometry of Kilauea Iki lava lake, Hawaii. Bull Volcanol 49:651–668

Helz RT, Banks NG, Heliker CT, Neal CA, Wolfe EW (1995) Comparative geothermometry of recent Hawaiian eruptions. J Geophys Res 100:17637–17657

Heslop SE, Wilson L, Pinkerton H, Head JW (1989) Dynamics of a confined lava flow on Kilauea Volcano, Hawaii. Bull Volcanol 51:415–432

Hon K, Kauahikaua JP, Denlinger R, Mackay K (1994) Emplacement and inflation of pāhoehoe sheet flows: observations and measurements of active lava flows on Kilauea Volcano, Hawaii. Geol Soc Am Bull 106:351–370

Hon K, Kauahikaua J, Mackay K (1993) Inflation and cooling data from pāhoehoe sheet flows on Kilauea Volcano. US Geol Survey Open-File Report 93–342A

Hoover SR, Cashman KV, Manga M (2001) The yield strength of subliquidus basalts; experimental results. J Volcanol Geotherm Res 107:1–18

Iverson R, LaHusen RG, Major JJ, Zimmerman CL (1994) Debris flow against obstacles and bends: dynamics and deposits. EOS, Trans Am Geophys Union 75:274

Jones AE (1943) Classification of lava-surfaces. Trans Am Geophys Union:265–268

Kauahikaua, JP, Margriter S, Lockwood J, Trusdell, F (1995) Application of GIS to the estimation of lava flow hazards on Mauna Loa Volcano, Hawai'i. AGU Monogr 92:315:325

Kauahikaua JP, Cashman KV, Clague DA, Champion DE, Hagstrum JT (2002) Emplacement of the most recent lava flows on Hualalai Volcano, Hawai'i. Bull Volcanol DOI 10.1007/s00445-001-0196-8

Kilburn CR (1981) Pahoehoe and aa lavas: a discussion and continuation of the model of Peterson and Tilling. J Volcanol Geotherm Res 11:373–382

Kilburn CRJ (1990) Surfaces of aa flow-fields on Mount Etna, Sicily; morphology, rheology, crystallization and scaling phenomena. In: Fink JH (ed) Lava flows and domes. Springer, Berlin Heidelberg New York, pp 129–156

Kilburn CRJ, Lopes RMC (1991) General patterns of flow field growth: aa and blocky lavas. J Geophys Res 96:19,712–719,732

Kilburn CRJ, Guest JE (1993) Aa lavas of Mount Etna, Sicily. In: Kilburn CRJ, Luongo G (eds) Active lavas. UCL Press, London, pp 73–106

Langlas C (1990) The people of Kalapana 1823–1950: a report of the Kalapana oral history project, pp 50

Lipman PW, Banks NG (1984) 'A'a flow dynamics, Mauna Loa 1984. In: Decker RW, Wright TL, Stauffer PH (eds) Volcanism in Hawai'i. US Geol Survey Prof Pap 1350, pp 1527–1567

Lockwood JP, Tilling RI, Holcomb RT, Klein F, Okamura AT, Peterson DW (1999) Magma migration and resupply during the 1974 summit eruptions of Kilauea Volcano, Hawaii. US Geol Survey Prof Pap 1613, 37 pp

Macdonald GA (1953) Pahoehoe, aa, and block lava. Am J Sci 251:169–191

Moore HJ, Kachadoorian R (1980) Estimates of lava-flow velocities using lava trees. Reports of Plan Geol Prog 1979–1980, pp 201–203

Moore HJ, Schaber GG (1975) An estimate of the yield strength of the Imbrium lava flows. Proc 6th Lunar Sci Conf. Pergamon Press, New York, pp 108–111

Nichols RL (1939) Viscosity of lava. J Geol 47:290–302

Peterson DW, Tilling RI (1980) Transition of basaltic lava from pāhoehoe to aa, Kilauea Volcano, Hawai'i: field observations and key factors. J Volcanol Geotherm Res 7:271–293

Philpotts AR, Shi J, Brustman C (1998) Role of plagioclase crystal chains in the differentiation of partly crystallized basaltic magma. Nature 395:343–346

Pinkerton H, Wilson L (1994) Factors controlling the lengths of channel-fed lava flows. Bull Volcanol 56:108–120

Polacci M, Cashman KV, Kauahikaua JP (1999) Textural characterization of the pāhoehoe-'a'a transition in Hawaiian basalt. Bull Volcanol 60:595–609

Pouchou J, Pichoir F (1991) Quantitative analysis of homogeneous or stratified microvolumes applying the model "PAP". In: Heinrich KFJ, Newbury DE (eds) Electron probe quantitation. Plenum Press, New York

Rowland SK, Walker GPL (1990) Pahoehoe and aa in Hawaii: volumetric flow rate controls the lava structure. Bull Volcanol 52:615–628

Rowland SK, Walker GPL (1987) Toothpaste lava: characteristics and origin of a lava structural type transitional between pahoehoe and aa. Bull Volcanol 49:631–641

Saar MO, Manga M, Cashman KV, Fermouw S (2001) Numerical models of the onset of yield strength in crystal-melt suspensions. Earth Planet Sci Lett 187:367–379

Sparks RSJ, Pinkerton H, Hulme G (1976) Classification and formation of lava levees on Mount Etna, Sicily. Geology 4:269–271

Stearns HT (1926) The Keaiwa or 1823 lava flow from Kilauea Volcano, Hawaii. J Geol 34:336–351

Swanson DA (1973) Pahoehoe flows from the 1969–1971 Mauna Ulu eruption, Kilauea Volcano, Hawaii. Geol Soc Am Bull 84:615–626

USGS (1981) Kau Desert quadrangle, Hawaii. 1:24,000. 7.5 minute series (topographic). Washington, DC

Wadge G, Young PAV, McKendrick IJ (1994) Mapping lava flow hazards using computer simulation. J Geophys Res 99:489–504

Wentworth CK, Macdonald GA (1953) Structures and forms of basaltic rocks in Hawai'i. US Geol Survey Bull 994, 98 pp

Wolfe EW, Neal CA, Banks NG, Duggan TJ (1988) Geologic observations and chronology of eruptive events. In: Wolfe EW (ed) The Puu Oo eruption of Kilauea Volcano, Hawaii: episodes 1 through 20, January 3, 1983, through June 8, 1984. US Geol Survey Prof Pap 1463, pp 1–99